**RESEARCH ARTICLE**

**Key Points:**

- The accuracy and predictive quality of age-depth models for tropical marine hemipelagic cores improves when bulk sediment composition is included
- The *BomDia* algorithm produces age-depth models with realistic accumulation rates, which co-vary with bulk sediment composition
- The *BomDia* algorithm uses a Monte Carlo approach to assess age-depth model uncertainty

**Correspondence to:**

F. J. C. Peeters,
f.j.c.peeters@vu.nl

**Author Contributions:**

**Conceptualization:** F. J. C. Peeters
**Formal analysis:** F. J. C. Peeters
**Investigation:** F. J. C. Peeters, H. J. L. van der Lubbe, P. Scussolini
**Methodology:** F. J. C. Peeters
**Resources:** F. J. C. Peeters, H. J. L. van der Lubbe, P. Scussolini
**Software:** F. J. C. Peeters
**Validation:** F. J. C. Peeters
**Visualization:** F. J. C. Peeters
**Writing – original draft:** F. J. C. Peeters
**Writing – review & editing:** F. J. C. Peeters, H. J. L. van der Lubbe, P. Scussolini

# Age-Depth Models for Tropical Marine Hemipelagic Deposits Improve Significantly When Proxy-Based Information on Sediment Composition Is Included

**F. J. C. Peeters[1]** , **H. J. L. van der Lubbe[1]** , **and P. Scussolini[2]**

[1]Department of Earth Sciences, Faculty of Science, Vrije Universiteit, Amsterdam, The Netherlands, [2]Institute for Environmental Studies (IVM), Vrije Universiteit Amsterdam, Amsterdam, The Netherlands

**Abstract** Accurate age-depth models for marine sediment cores are crucial for understanding paleo-oceanographic and -climatic changes derived from these archives. To date, information on bulk sediment composition is largely ignored as a potential source of information to improve age-depth models. In this study, we explore how bulk sediment composition can be qualitatively used to improve age-depth models. We developed the *BomDia* algorithm, which produces age-depth models with realistic sediment accumulation rates that co-vary in harmony with the bulk sediment composition. We demonstrate that changes in the marine versus terrigenous sediment deposition, based on bulk sediment composition, can be used to significantly improve age-depth models of hemipelagic marine deposits. Based on two marine records—each containing more than 20 radiocarbon (AMS $^{14}$C) dated levels—we show that the mean error of prediction of unused AMS $^{14}$C ages significantly improves from 3.9% using simple linear interpolation, to 2.4% ($p = 0.003$), when bulk sediment composition is included. The *BomDia* age-depth modeling approach provides a powerful statistical tool to assess the validity of age control points used and also may assist in the detection of hiatuses. Testing and further development of the *BomDia* algorithm may be needed for application in depositional settings other than tropical hemipelagic.

**Plain Language Summary** The age-depth relationship in a marine sediment core is known as an age-depth model. To build an age-depth model, that is to produce a continuous age-depth relationship, an accurate and precise prediction of ages in between age control points is needed. A new algorithm, which includes information on the bulk sediment composition in the prediction of ages, has been developed and tested for this purpose. The calcium carbonate content of the sediments is calibrated versus the log ratio of titanium and calcium as obtained from resolution X-ray fluorescence and used as model input for bulk sediment composition. We tested the algorithm using data from two tropical hemipelagic cores and find that the algorithm, which we refer to as *BomDia* ("a good dynamic interpolation algorithm"), produces robust age-depth models with predictive power and realistic sedimentation rates that co-vary with sediment composition. Further application and testing of the algorithm to a wider variety of other than tropical hemipelagic sedimentary settings is recommended.

## 1. Introduction

### 1.1. Age-Models for Marine Sediments

Marine hemipelagic sediment cores provide valuable high-resolution paleo-climatic and -oceanographic archives of both past marine changes as well as past terrestrial climate dynamics of the nearby continent. To make use of the paleo-oceanographic and -climatic proxy signals recorded in marine sediments, the sediment depth in core must be converted into age: a procedure that is referred to as age-depth modeling (e.g., Blaauw, 2010). A robust age-depth model has realistic sediment accumulation rates (*SARs*) and low age uncertainties. A reliable and accurate age-depth model, with low age uncertainty, is a prerequisite for meaningful interpretation and understanding of the regional temporal paleoclimatic signal and its potential spatiotemporal tele-connections. Age control of sedimentary archives is obtained either directly, for example, by using radiometric methods such as Accelerator Mass Spectrometer radiocarbon dating (AMS $^{14}$C), or indirectly by aligning characteristic events in proxy records (e.g., $\delta^{18}$O benthic records) to other records with trusted chronologies and assuming synchronicity of these events (Govin et al., 2015; Lisiecki & Raymo, 2005). In this study, we use the term "age control points" (ACPs) for

direct age assessments (e.g., AMS ^{14}C or dated ash-layers) and for tuned—and hence indirect—age assessments obtained via proxy alignment or "wiggle matched" events, we use the term tie-point.

To establish an age-depth relationship for a given record, various methods and algorithms have been developed over the past decades (Blaauw, 2010; Blaauw & Christen, 2011; Bronk Ramsey, 2009; Lougheed & Obrochta, 2019; Trachsel & Telford, 2017). Although these algorithms are well designed to estimate and potentially reduce age-depth model uncertainty, a potential valuable source of information, which is the bulk composition of the sediment, has not been considered thus far. In this study, we investigate how bulk sediment composition can provide useful information on how ACPs and tie-points are connected. The study is composed of two parts: first we test if prediction of AMS ^{14}C ages performs better if bulk sediment composition is included versus prediction of these ages using linear interpolation, then we show how a full core aged-depth model can be constructed and assess age-depth model uncertainty using a Monte Carlo approach.

### 1.2. Over-Tuned Age-Depth Models and Unrealistic Accumulation Rates

The age of marine sediments younger than ~50 ka is generally well-constrained through the use of AMS ^{14}C radiocarbon dating. Age control for older sediments, however, often relies on strategies of tuning events to various types of reference chronologies, including, for example, other marine sediment proxy time series, ice cores, or speleothems. This tuning strategy requires the assumption of synchronicity, or known time offset, between climatic events recorded and their correlative counterpart in distant archives. This alignment practice may result in potentially unrealistic age-depth models (for discussion see e.g., Blaauw, 2012; Govin et al., 2015; Telford et al., 2004; Trachsel & Telford, 2017). Although it appears intuitively useful to use as many tie-points as possible—to optimize the fit between the investigated and target time series—one must realize that with each added tie-point a new assumption about synchronicity is made. The use of too many tie-points, is known as over-tuning. It introduces noise (e.g., irregularities) into the age-depth model and may produce erroneous chronologies (Martinson et al., 1987). Furthermore, once two proxy records are tuned to one another, both chronologies cannot be used to infer synchronicity, leads or lags of climatic events therein. This is regrettable, as a tuned record without independent validation of the assumption of tie-point synchronicity largely loses its valuable and independent paleoclimate information or, even worse, artificially implies non-existing, but visually pleasing, synchronous paleoclimate tele-connections.

A second problem that afflicts age-depth modeling relates to the necessary step of interpolating between the ACPs, required to obtain a continuous chronology for a given record. This is done by either using linear/spline interpolations or through the use of (Bayesian) age-depth model algorithms (e.g., Blaauw & Christen, 2011; Bronk Ramsey, 2009; Lougheed & Obrochta, 2019). In the most common method of a classic linear interpolation, the *SARs* are constant between two successive ACPs (or tie-points). As such, the timing and duration of certain paleoclimatic events between ACPs (or tie-points) may not agree well with the reference chronology and/or other paleoclimate archives. Iteratively including or excluding ACPs during age-depth model construction, to meet the goal of aligning events to one-another, is a time-consuming exercise, with the potential risk of aligning events that in reality are asynchronous. In literature, several examples may be found of records which are over-tuned for the sake of a desired or expected agreement between the record under investigation and the reference chronology (e.g., see Blaauw, 2012). Over-tuning, however, may be avoided through modeling *SARs* in line with sediment composition, hence reflecting the dynamics of the depositional environment.

### 1.3. Previous Studies

In some previous studies, it was proposed to use sedimentological or micropaleontological information to improve age-depth models. Herterich and Sarnthein (1984), for example, assumed a fairly constant accumulation rate of Saharan dust for a core in the equatorial Atlantic to assess accumulation rates. The approach has not been applied widely and there is evidence that the main assumption is invalid given that dust fluxes varied considerably over time (Skonieczny et al., 2019). A micropaleontological approach to estimate ages between control points was proposed by Crundwell (2016), who used a uniform accumulation rate of foraminifera, as opposed to a uniform bulk *SAR*, to estimate ages between ACPs. Although Crundwell's approach appears to improve the age-depth model compared to linear interpolation, the method requires microscopic study of samples, which may involve a time-consuming analysis.
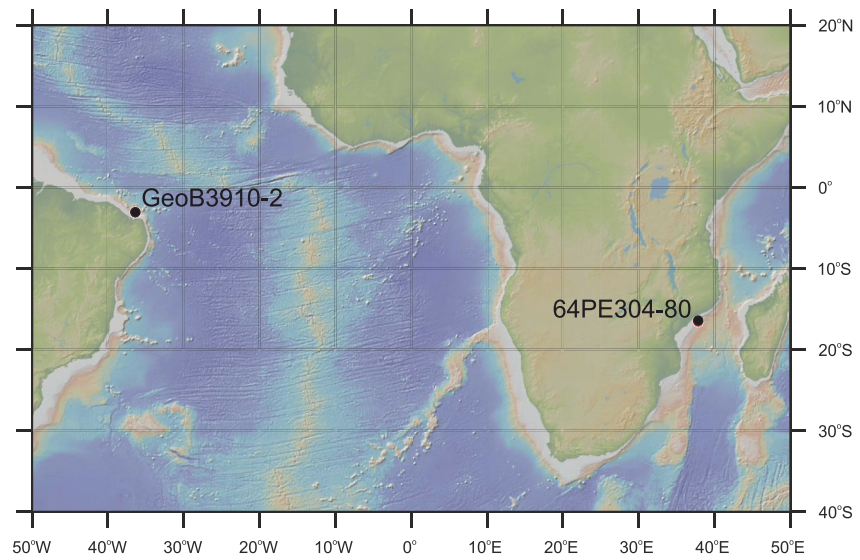
**Figure 1.** Core locations investigated in this study. Details for core GeoB3910-2 (2,362 m water depth) can be found in Jaeschke et al. (2007b) and for core 64PE304-80 (1,329 m water depth) in van der Lubbe et al. (2016, 2014).

### 1.4. Bulk Sediment Composition

The idea that bulk sediment composition, in combination with high-resolution XRF core scanning, may be a useful source of information for improving age-depth models, has received little attention and hence serves as a motivation for this study. For cores collected above the carbonate compensation depth, the calcium carbonate weight percent ($CaCO_3$ wt.%) of marine sediments is probably the most characteristic measure of bulk sediment composition. For hemipelagic records, it correlates generally very well with the log(Ti/Ca) and log(Fi/Ca) ratios as obtained by XRF core scanning (e.g., Arz et al., 1998; Chiessi et al., 2021; Hodell et al., 2013; van der Lubbe et al., 2014). Our hypothesis in this study postulates that if proxy-based bulk sediment composition is included in the age-depth modeling procedure, this will result in more realistic age-depth models with lower age uncertainty and higher predictive power.

To test our hypothesis, we use data from two published records: the first one being core 64PE304-80 from the Mozambican continental margin (van der Lubbe et al., 2016) and the second one, core GeoB3910-2 (Jaeschke et al., 2007b), from the northeast Brazilian continental slope (Figure 1). These sediment cores are retrieved from continental margins, which receive relatively high terrigenous inputs, which varied strongly related to past shifts in regional runoff and rainfall patterns (Jaeschke et al., 2007b; van der Lubbe et al., 2016, 2014). Both cores are well suited for testing our hypothesis as they have a hemipelagic accumulation history and an excellent chronology based upon a high density of AMS $^{14}$C radiocarbon dates (each $n > 20$).

## 2. Rationale and Research Approach

### 2.1. Sediment Composition and Accumulation Rate

Marine hemipelagic sediments represent a mixture of marine biogenic components (foraminifera, coccoliths, pteropods, diatoms, and radiolarians) and clay and silt-sized lithogenic components predominantly of terrestrial origin. For sediments on continental margins in tropical regions, the non-marine terrigenous fraction mostly originates from fluvial and aeolian processes (e.g., Fütterer, 2006). Non-destructive X-ray fluorescence core scanning (XRF) provides high-resolution elemental records of bulk sediment in marine cores (Weltje & Tjallingii, 2008). The terrigenous component in marine sediments is strongly reflected in elements like titanium (Ti) or iron (Fe), whereas the biogenic, dominantly pelagic, carbonate component is reflected by calcium (Ca) (Hennekam & de Lange, 2012). Subsequently, the ratio, or preferentially the log ratio (Weltje & Tjallingii, 2008), of Ti or Fe over Ca mirrors the relative contribution of terrestrial components over the marine carbonate fraction and correlates generally very well with the calcium carbonate weight percent ($CaCO_3$ wt.%) in marine sediments (Figure 2). It is well documented that carbonate-rich pelagic sediments, as for example, found on mid-oceanic ridges have
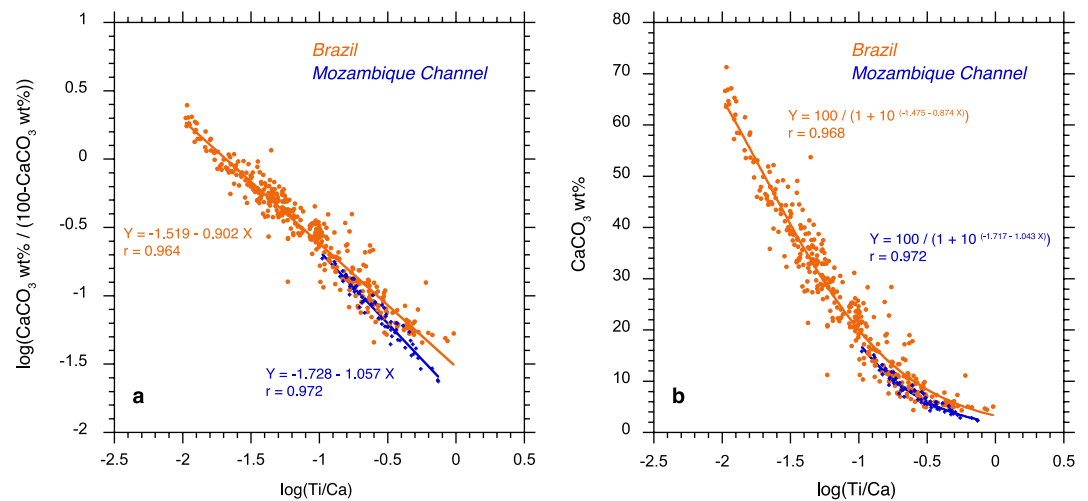
**Figure 2.** Scatter plots and regression lines for (a) $\log(CaCO_3/(100 - CaCO_3))$ versus $\log(Ti/Ca)$ (cf. Weltje & Tjallingii, 2008) and (b) $CaCO_3$ wt.% versus $\log(Ti/Ca)$. For sediments from the northeast Brazil margin, we use data of core MD09-3246 (890 m water depth) (Scussolini et al., 2014) and for the Mozambican margin, we use data of core GIK16160-3 (van der Lubbe, 2022b). The values of the regression parameters for both equation types are very similar to one another.

accumulated much slower compared clay-rich sediments on continental margins near river outflows (Olson et al., 2016). Hence, at a given location, carbonate-rich sediments that are accompanied with lower $\log(Ti/Ca)$ and $\log(Fe/Ca)$ ratios, typically reflect low *SARs* as a result of less input of terrigenous components.

## 2.2. Core Sites

The aforementioned marine records are derived from the tropical Atlantic Ocean on the continental margin of north-eastern Brazil, GeoB3910-2 (2,362 m) (Jaeschke et al., 2007b) and the other from the western tropical Indian Ocean 64PE304-80 (1,329 m; Figure 1). The lithology of both hemipelagic records is composed of a mixture of clays and marine pelagic carbonate, predominantly foraminifera and calcareous nanno-fossils. Both records have been scanned using an elemental XRF core scanner, exhibiting a high variability in $\log(Ti/Ca)$ ratios in both records. High $\log(Ti/Ca)$ values are consistently associated with high rainfall and river runoff and hence associated with high input of terrigenous derived compounds (Arz et al., 1998; Jaeschke et al., 2007b; Schefuss et al., 2011; van der Lubbe et al., 2014). Core site GeoB3910-2 is under the influence of the river and tributary systems of the Nordeste region, which sediment discharges are presently low due to the relatively dry climate of the hinterland. Large pulses of riverine sediment discharges, however, have been linked to southwards shifts of the Intertropical Convergence Zone (Arz et al., 1998, 1999; Behling et al., 2000; Jaeschke et al., 2007b). Variability in riverine discharge and rainfall has been also inferred from site 64PE304-80, which experienced a more persistent sediment discharge from the large Zambezi catchment that is situated at the southernmost extent of the ITCZ (Schefuss et al., 2011; van der Lubbe et al., 2016, 2014). Both records are densely AMS $^{14}$C dated; the GeoB3910-2 record contains 24 dated levels and the 64PE340-80 record contains 22 dates of which 10 were projected from core GIK16160-3 from the same site (van der Lubbe et al., 2014). Given the limit of the AMS $^{14}$C dating, we here only consider sediments younger than ~50 ka. We discuss the details of the experimental design associated to the testing of this hypothesis in the section below.

## 2.3. Experimental Design

The experimental design involves prediction of AMS $^{14}$C calibrated calendar ages using two different age-depth model methods and—for each core—two independent sets of AMS $^{14}$C dates. The first age-depth model method uses simple linear interpolation and for the second method we use our newly developed algorithm (see Section 3.3), which utilizes information on bulk sediment composition to interpolate between ACPs (see Section 3 for details). The experimental setup involves evaluation of the accuracy in the prediction of ages using both methods. For each core, we split the total number of AMS $^{14}$C dates in two subsets. For core GeoB3910-2 we create an "ODD" and

an "EVEN" subset. The "ODD" set includes the top age and then the third, fifth, etc. AMS ^{14}C age, the "EVEN" subset includes the top age, the second, fourth, etc. AMS ^{14}C age. For core 64PE304-80 the first subset consists of the radiocarbon ages measured on core 64PE304-80 and the second subset consists of radiocarbon ages from core GIK16160-3, which were precisely transferred onto the depth scale of core 64PE304-80 through detailed comparison of the log(Ti/Ca) curves of both cores (van der Lubbe et al., 2014). For each subset, we thus produce two age-depth models: a linear age-depth model and an age-depth model which includes the sediment composition. In the final step, the ages at the depth levels of the unused AMS ^{14}C subset are predicted and, as such, we can test which interpolation method more accurately predicts the unused ages of the other subset. The accuracy of the prediction is expressed as the absolute difference between the predicted and the observed median AMS ^{14}C age expressed relative to the median AMS ^{14}C age (Equation 1):

$$\text{rel. error of prediction} = \frac{\left| \text{model predicted age} - \text{radiocarbon age} \right|}{\text{radiocarbon age}} \cdot 100 \tag{1}$$

In the null hypothesis, it is stated that both methods of interpolation perform equally well and the alternative hypothesis states that prediction of unused ages improves when bulk sediment composition is taken into account. A one-sided paired student $t$-test is used to detect if there is a significant improvement in the relative error of prediction for the method including sediment composition. Rejection of the null-hypothesis is taken as evidence that including bulk sediment composition significantly improves the age-depth modeling.

## 3. Methods

### 3.1. Radiocarbon Dating

As explained above, we utilize AMS ^{14}C calendar ages to produce various age models for cores GeoB3910-2 and for core 64PE304-80. Published AMS ^{14}C radiocarbon dates were re-calibrated to calendar ages using MatCal software (Lougheed & Obrochta, 2016), the IntCal20 curve (Reimer et al., 2020) and applying a marine reservoir age correction of $500 \pm 50$ yr for both records. The calendar ages are reported in conventional "kiloyear-before-present" (ka BP) notation (Table 1).

### 3.2. Bulk Sediment Composition

In this study, we use $CaCO_3$ wt.% as a proxy for bulk sediment composition. The $CaCO_3$ wt.% of sediments from the Mozambican and Brazilian margins has been measured on nearby cores MD09-3246 (Scussolini et al., 2014) and core GIK16160-3 (van der Lubbe et al., 2014). The $CaCO_3$ wt.% was measured using a CARLO ERBA Elemental Analyzer and LECO TGA-601 instrument at the Vrije Universiteit Amsterdam on ∼1 cm[3] of dry sediment (Scussolini et al., 2014; van der Lubbe et al., 2014). In Figure 2, we present scatter plots and correlations between log(Ti/Ca) and $CaCO_3$ wt.% as obtained for sediments from the northeast Brazilian and Mozambican margin. Sediments with low log(Ti/Ca) ratios correlate with high $CaCO_3$wt.%. Following Weltje and Tjallingii (2008), a linear relationship exists between log(Ti/Ca) and $\log(CaCO_3 \text{ wt.\%}/(100 - CaCO_3 \text{ wt.\%}))$. We have applied this regression and show the results in Figure 2a. In addition, we also solved their equation to directly regress $CaCO_3$ wt.% versus log(Ti/Ca) (Figure 2b). The nonlinear equation regression to obtain $CaCO_3$ wt.% from log(Ti/Ca) is:

$$CaCO_3 \text{ wt\%} = \frac{100}{1 + 10^{(a+b\cdot\log(\text{Ti/Ca}))}} \tag{2}$$

For the Brazilian sediments, we obtained $a = -1.475$ and $b = -0.874$ and for the Mozambique Channel sediments $a = -1.717$ and $b = -1.043$. Both sigmoidal regressions have a correlation coefficient of $r = 0.97$ (Figure 2b).

### 3.3. The "*BomDia*" Algorithm

The $CaCO_3$ wt.% proxy-record is used to calculate *SARs* between two consecutive ACPs (or tie-points), which we here will refer to as "a segment" and which has been XRF-scanned at sampling resolution $\Delta z$, which will refer to as "an increment". In this study, $\Delta z$ equals 1 cm for both cores. Below we will explain how the *SARs* for a given segment, sampled at resolution $\Delta z$, is calculated as a function of the bulk sediment composition.

**Table 1**
*Age Control Points and Model Predicted Ages for Cores GeoB3910-2 and 64PE304-80*

| Core | Depth [cmbsf] | Type | Lab number | c14 age [yr BP] | 1 sigma | Calendar age max. 95% [ka BP] | Calendar age median [ka BP] | Calendar age min. 95% [ka BP] | Predicted age linear [kyr] (this study) | Abs. rel. offset from median age (%) | Predicted age *BomDia* [kyr] (this study) | Abs. rel. offset from median age (%) |
|---|---|---|---|---|---|---|---|---|---|---|---|---|
| GeoB3910-2 (ODD) | 1 | 14C (Jaeschke et al., 2007a, 2007b) | KIA6800 | 565 | 30 | 0.277 | 0.143 | 0.009 | | | | |
| GeoB3910-2 (ODD) | 23 | 14C (Jaeschke et al., 2007a, 2007b) | KIA6798 | 6,160 | 40 | 6.622 | 6.464 | 6.306 | 5.718 | 11.5 | 5.883 | 9.0 |
| GeoB3910-2 (ODD) | 58 | 14C (Jaeschke et al., 2007a, 2007b) | KIA6815 | 10,090 | 60 | 11.184 | 10.943 | 10.701 | 10.809 | 1.2 | 11.420 | 4.4 |
| GeoB3910-2 (ODD) | 88 | 14C (Jaeschke et al., 2007a, 2007b) | KIA6813 | 12,840 | 110 | 14.962 | 14.507 | 14.052 | 13.964 | 3.7 | 14.641 | 0.9 |
| GeoB3910-2 (ODD) | 113 | 14C (Jaeschke et al., 2007a, 2007b) | KIA25824 | 14,000 | 70 | 16.557 | 16.282 | 16.007 | 16.260 | 0.1 | 16.459 | 1.1 |
| GeoB3910-2 (ODD) | 173 | 14C (Jaeschke et al., 2007a, 2007b) | KIA6811 | 20,000 | 170 | 23.819 | 23.435 | 23.050 | 22.565 | 3.7 | 22.996 | 1.9 |
| GeoB3910-2 (ODD) | 193 | 14C (Jaeschke et al., 2007a, 2007b) | KIA6808 | 22,480 | 220 | 26.905 | 26.384 | 25.862 | 25.668 | 2.7 | 24.983 | 5.3 |
| GeoB3910-2 (ODD) | 213 | 14C (Jaeschke et al., 2007a, 2007b) | KIA25821 | 25,130 | 260 | 29.536 | 28.822 | 28.107 | 28.290 | 1.8 | 28.850 | 0.1 |
| GeoB3910-2 (ODD) | 238 | 14C (Jaeschke et al., 2007a, 2007b) | KIA6806 | 28,280 | 430 | 33.090 | 32.102 | 31.113 | 31.315 | 2.4 | 31.090 | 3.1 |
| GeoB3910-2 (ODD) | 328 | 14C (Jaeschke et al., 2007a, 2007b) | KIA6804 | 38,600 | 1,480 | 45.129 | 42.789 | 40.449 | 41.535 | 2.9 | 40.831 | 4.6 |
| GeoB3910-2 (ODD) | 373 | 14C (Jaeschke et al., 2007a, 2007b) | KIA21890 | 44,480 | 1,250 | 49.799 | 47.158 | 44.516 | 46.041 | 2.4 | 47.371 | 0.5 |
| GeoB3910-2 (ODD) | 435 | Tie-point (Waelbroeck et al., 2019) | - | - | - | 55.062 | 54.236 | 53.410 | 53.832 | 0.7 | 54.546 | 0.6 |
| GeoB3910-2 (EVEN) | 13 | 14C (Jaeschke et al., 2007a, 2007b) | KIA6799 | 3,930 | 35 | 3.840 | 3.667 | 3.493 | 3.716 | 1.3 | 3.664 | 0.1 |
| GeoB3910-2 (EVEN) | 38 | 14C (Jaeschke et al., 2007a, 2007b) | KIA7225 | 8,430 | 40 | 8.987 | 8.795 | 8.602 | 8.384 | 4.7 | 8.799 | 0.0 |
| GeoB3910-2 (EVEN) | 73 | 14C (Jaeschke et al., 2007a, 2007b) | KIA6814 | 10,940 | 70 | 12.664 | 12.319 | 11.974 | 12.725 | 3.3 | 12.339 | 0.2 |
| GeoB3910-2 (EVEN) | 103 | 14C (Jaeschke et al., 2007a, 2007b) | KIA25825 | 13,550 | 70 | 15.892 | 15.609 | 15.326 | 15.572 | 0.2 | 15.675 | 0.4 |
| GeoB3910-2 (EVEN) | 148 | 14C (Jaeschke et al., 2007a, 2007b) | KIA6812 | 15,780 | 110 | 18.799 | 18.539 | 18.279 | 20.455 | 10.3 | 18.009 | 2.9 |
| GeoB3910-2 (EVEN) | 183 | 14C (Jaeschke et al., 2007a, 2007b) | KIA25822 | 20,580 | 150 | 24.546 | 24.176 | 23.805 | 24.910 | 3.0 | 25.631 | 6.0 |
| GeoB3910-2 (EVEN) | 200 | 14C (Burckel et al., 2015) | B15-1 | 22,850 | 130 | 27.086 | 26.712 | 26.338 | 27.237 | 2.0 | 27.116 | 1.5 |
| GeoB3910-2 (EVEN) | 233 | 14C (Jaeschke et al., 2007a, 2007b) | KIA25820 | 27,160 | 310 | 31.249 | 30.717 | 30.185 | 31.446 | 2.4 | 31.349 | 2.1 |
| GeoB3910-2 (EVEN) | 268 | 14C (Jaeschke et al., 2007a, 2007b) | KIA22411 | 30,860 | 430 | 35.723 | 34.906 | 34.088 | 35.664 | 2.2 | 36.421 | 4.3 |
| GeoB3910-2 (EVEN) | 348 | 14C (Jaeschke et al., 2007a, 2007b) | KIA21829 | 41,000 | 820 | 44.867 | 43.745 | 42.622 | 44.731 | 2.3 | 44.815 | 2.4 |
| GeoB3910-2 (EVEN) | 400 | Tie-point (Waelbroeck et al., 2019) | - | - | - | 49.948 | 48.520 | 47.092 | 50.240 | 3.5 | 48.445 | 0.2 |

**Table 1**
*Continued*

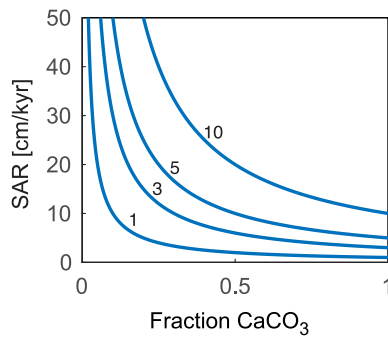| Core | Depth [cmbsf] | Type | Lab number | $c14$ age [yr BP] | 1 sigma | Calendar age max. 95% [ka BP] | Calendar age median [ka BP] | Calendar age min. 95% [ka BP] | Predicted age linear [kyr] (this study) | Abs. rel. offset from median age (%) | Predicted age *BomDia* [kyr] (this study) | Abs. rel. offset from median age (%) |
|---|---|---|---|---|---|---|---|---|---|---|---|---|
| GeoB3910-2 (EVEN) | 453 | Tie-point (Waelbroeck et al., 2019) | - | - | - | 57.220 | 56.564 | 55.908 | | | | |
| GIK16160-3 (projected) | 253 | $^{14}$C (van der Lubbe et al., 2014) | KIA41418 | 9,330 | 50 | 10.180 | 9.894 | 9.608 | 9.352 | 5.5 | 10.534 | 6.5 |
| GIK16160-3 (projected) | 283 | $^{14}$C (van der Lubbe et al., 2014) | KIA41419 | 10,560 | 60 | 11.872 | 11.573 | 11.273 | 10.493 | 9.3 | 12.182 | 5.3 |
| GIK16160-3 (projected) | 306 | $^{14}$C (van der Lubbe et al., 2014) | KIA41420 | 11,620 | 70 | 13.170 | 13.003 | 12.835 | 11.367 | 12.6 | 13.159 | 1.2 |
| GIK16160-3 (projected) | 358 | $^{14}$C (van der Lubbe et al., 2014) | KIA41421 | 13,070 | 70 | 15.217 | 14.783 | 14.349 | 13.344 | 9.7 | 15.252 | 3.2 |
| GIK16160-3 (projected) | 388 | $^{14}$C (van der Lubbe et al., 2014) | KIA41422 | 13,590 | 70 | 15.968 | 15.680 | 15.391 | 14.484 | 7.6 | 16.080 | 2.6 |
| GIK16160-3 (projected) | 424 | $^{14}$C (van der Lubbe et al., 2014) | KIA43168 | 14,269 | 68 | 16.986 | 16.698 | 16.409 | 15.853 | 5.1 | 16.748 | 0.3 |
| GIK16160-3 (projected) | 568 | $^{14}$C (van der Lubbe et al., 2014) | KIA41424 | 17,170 | 120 | 20.493 | 20.076 | 19.659 | 20.247 | 0.9 | 20.277 | 1.0 |
| GIK16160-3 (projected) | 781 | $^{14}$C (van der Lubbe et al., 2014) | KIA43169 | 23,749 | 192 | 27.778 | 27.506 | 27.234 | 28.209 | 2.6 | 27.840 | 1.2 |
| GIK16160-3 (projected) | 968 | $^{14}$C (van der Lubbe et al., 2014) | KIA43179 | 32,754 | 589 | 38.699 | 37.061 | 35.422 | 36.455 | 1.6 | 36.356 | 1.9 |
| 64PE304-80 | 10 | $^{14}$C (van der Lubbe et al., 2014) | KIA45243 | 450 | 30 | 0.261 | 0.144 | 0.027 | | | | |
| 64PE304-80 | 188 | $^{14}$C (van der Lubbe et al., 2014) | KIA43827 | 6,145 | 35 | 6.600 | 6.450 | 6.300 | 7.286 | 13.0 | 6.701 | 3.9 |
| 64PE304-80 | 223 | $^{14}$C (van der Lubbe et al., 2014) | KIA43829 | 7,940 | 40 | 8.384 | 8.212 | 8.040 | 8.690 | 5.8 | 8.427 | 2.6 |
| 64PE304-80 | 488 | $^{14}$C (van der Lubbe et al., 2014) | KIA45244 | 15,400 | 70 | 18.603 | 18.286 | 17.969 | 18.199 | 0.5 | 17.898 | 2.1 |
| 64PE304-80 | 515 | $^{14}$C (van der Lubbe et al., 2014) | KIA45245 | 16,360 | 80 | 19.417 | 19.168 | 18.919 | 18.833 | 1.7 | 18.662 | 2.6 |
| 64PE304-80 | 605 | $^{14}$C (van der Lubbe et al., 2014) | KIA45246 | 17,870 | 110 | 21.367 | 21.000 | 20.632 | 21.367 | 1.7 | 21.290 | 1.4 |
| 64PE304-80 | 659 | $^{14}$C (van der Lubbe et al., 2014) | KIA43821 | 20,530 | 140 | 24.462 | 24.124 | 23.786 | 23.250 | 3.6 | 23.197 | 3.8 |
| 64PE304-80 | 834 | $^{14}$C (van der Lubbe et al., 2014) | KIA43822 | 26,210 | 270 | 30.726 | 29.983 | 29.240 | 30.214 | 0.8 | 30.281 | 1.0 |
| 64PE304-80 | 875 | $^{14}$C (van der Lubbe et al., 2014) | KIA43823 | 28,360 | 340 | 32.957 | 32.074 | 31.191 | 32.309 | 0.7 | 32.280 | 0.6 |
| 64PE304-80 | 935 | $^{14}$C (van der Lubbe et al., 2014) | KIA45247 | 30,200 | 370 | 35.041 | 34.172 | 33.303 | 35.375 | 3.5 | 35.237 | 3.1 |
| 64PE304-80 | 1.005 | $^{14}$C (van der Lubbe et al., 2014) | KIA43824 | 34,640 | 740 | 40.855 | 39.014 | 37.172 | | | | |
| 64PE304-80 | 1.071 | $^{14}$C (van der Lubbe et al., 2014) | KIA43825 | 37,740 | 1,100 | 43.248 | 41.669 | 40.090 | | | | |
| | | | | | | | | | Average | 3.9 | | 2.4 |
| | | | | | | | | | St.dev. | 3.5 | | 2.1 |

**Figure 3.** Sediment accumulation rate (*SAR*) as a function of the calcium carbonate fraction (fCaCO$_3$) for different values of the carbonate accumulation rate parameter, indicated by numbers above lines. The lines follow the relationship of Equation 3.

First of all, it is important to realize that CaCO$_3$ wt.% is known at the discrete depth levels of the XRF sampling resolution. Hence, we first calculate a mean CaCO$_3$ wt.% value for the increments $\Delta z$. Let's assume we have $n$ increments in a given segment for which we wish to calculate the incremental *SAR* values. To do so, we first convert the discrete CaCO$_3$ wt.% values to mean CaCO$_3$ wt.% for each of the increments in the segment and we express these values as a mean fraction $\left( \left( \overline{f\mathrm{CaCO_3}} \right)_i \right)$. Then, we use an inverse relationship to model *SAR* as a function of $\left( \overline{f\mathrm{CaCO_3}} \right)_i$ and a single scaling parameter, which we here refer to as the carbonate accumulation rate (*CAR*). We then calculate the *SAR* for increment i as:

$$SAR_i = CAR / \left( \overline{f\mathrm{CaCO_3}} \right)_i \qquad (3)$$

The relationship is graphically illustrated in Figure 3. The value of the *CAR* parameter is constant within a given segment with total time-span *T*. For clarity, *T* equals the age at the base minus the age at the top of the segment.

The value of the *CAR* parameter is calculated using $\Delta z$, *T* and the sum of the mean carbonate fractions of all increments in a given segment. The *CAR* value is equal to:

$$CAR = \frac{\Delta z}{T} \cdot \sum_{i=1}^{n} \left( \overline{f\mathrm{CaCO_3}} \right)_i \qquad (4)$$

In practice, the *CAR* value (Equation 4) is calculated first and then used in Equation 3 to calculate *SAR* values for each of the increments in a given segment.

The *BomDia* ("*a good Dynamic Interpolation Algorithm*") algorithm "*BomDia.m*" is coded and tested in MATLAB®, R2020a, The MathWorks, Inc., Natick, Massachusetts, United States. No additional toolboxes are required. The algorithm requires a four-column array for the input of the ACPs listing depth in the first column, followed by three columns listing lower age boundary, median (or mean) age and upper age boundary of the ACPs. In addition a two-column input array with ascending equal spaced depth in the first column and CaCO$_3$ wt.% (here inferred from log(Ti/Ca)) in the second column, is required to run the algorithm. The full core age-depth model is obtained by stacking the age-depth models for the individual segments. Since for each core segment a unique *CAR* value is calculated (Equation 4), the function "*getcar.m*" is called several times from the main script. The *CAR* parameter values are expected to vary moderately between core segments as a result of past variation in pelagic carbonate production, sediment compaction processes or coring disturbances and, to some extent, dating uncertainty in ACPs. Since the *CAR* parameter is expected to vary gradually and minimally with depth in the core, the downcore evolution of the *CAR* parameter values may be used to detect age-depth model irregularities, resulting from coring disturbance, hiatuses and/or outlier ACPs. In this context, an anomalous low segment value for *CAR* may point to decreased past carbonate production or a hiatus. An anomalous high segment *CAR* value, however, may point to increased carbonate production or core stretching. The statistical distribution (histogram) of the *CAR* segment values and the down-core evolution are considered to provide useful tool in the validation of the age-depth model.

### 3.4. Assessing *BomDia* Age-Depth Model Uncertainties Using Monte Carlo Simulation

The *BomDia* algorithm provides a robust interpolation to estimate ages between ACPs. To assess age-depth model uncertainty, however, the uncertainty in the ACPs must be included. We here use a Monte Carlo approach to produce a large number (*nsim*) of age-depth model simulations, by randomly generating new ACP series from the 3-sigma uncertainty intervals of the ACPs. Random ACP series containing age reversals are removed during the selection process and replaced by a new ACP series containing no age reversals. Once the required number of random ACPs has been generated, *BomDia* generates *nsim* age-depth models from which a small sub-set of "best age-depth models" is isolated. The sub-set selection of size "*nbest*" is based upon the criterium of lowest variability in the *CAR* parameter. Prior to running the script, the user inputs a number for *nsim* and *nbest*. In this study we use *nsim* = 500,000 and *nbest* = 30.

## 4. Results

### 4.1. Core GeoB3910-2

For core GeoB3910-2, the 21 AMS $^{14}$C dates (Burckel et al., 2015; Jaeschke et al., 2007b) and three additional tie-points for radiocarbon free sediments older than ~47 ka (Waelbroeck et al., 2019) are used two create two sets of ACPs to develop two independent age-depth models, one using linear and the other using nonlinear "*BomDia*" interpolation (Table 1, Figure 4). As explained above, we refer to these models as the "GeoB3910-2-ODD" and the "GeoB3910-2-EVEN" age-depth models (Figures 4b and 4c). The ODD age-depth model is used to predict ages from the EVEN ACP set and vice versa. The overall average relative error of prediction, for both the ODD and EVEN sets together is 3.1% for the linear model predictions and 2.3% for the *BomDia* predictions, thus indicating a better performance for the latter. Since the distribution of the residuals, expressed as the percent difference between predicted and median calendar age, is not normally distributed (all values are positive and the distribution is skewed positively), we use a one-sided paired *t*-test to test if there is an improvement of the *BomDia* method compared to the linear interpolation method. This yields a *t*-value of −1.39 (degrees of freedom (*d.f.*) = 21) and a *t*-probability of $p = 0.090$. Since $p < 0.1$, we conclude that the result is result significant at the 90% confidence level.

### 4.2. Core 64PE304-80

For core 64PE304-80, we also use two subsets of ACPs to develop two independent age-depth models for each set of ACPs (Table 1, Figure 5). For this core, a set of 12 AMS $^{14}$C dates is available. In addition, a second set of 9 AMS $^{14}$C dates is available from adjacent core GIK16160-3. These AMS $^{14}$C ages were projected onto core 64PE304-80 with aid of the comparable XRF log(Ca/Ti) records (van der Lubbe et al., 2014). Similar to our approach for core GeoB3910-2, we use both ACP sub-sets to produce two independent age-depth models and to predict ages from the other ACP sub-set using linear and *BomDia* interpolation (Figure 5). Combining the results for both AMS $^{14}$C sub-sets, the overall relative error of prediction for the linear models is 4.8% and for the *BomDia* age-depth models the relative error of prediction is 2.5%. A paired *t*-test is used to assess the difference in prediction between the two methods. The test yields a *t*-value of −2.63 (*d.f.* = 17) and a *t*-probability of $p = 0.009$, indicating the result is significant at the 99% confidence level ($p < 0.01$).

### 4.3. Better Age-Depth Models Using *BomDia* Interpolation

By combining the results from both cores GeoB3910-2 and 64PE304-80, we arrive at an overall relative error of prediction of 3.9% for the linear interpolation predictions and 2.4% for *BomDia* predictions (Table 1). A paired *t* test ($n = 40$) for all data pairs for both cores, yields a *t*-value of −2.884 (D.F. = 39) and a *t*-probability of $p = 0.003$, indicating the result is highly significant. Hence, we can reject the null hypothesis and conclude that *BomDia* age-depth models, which take sediment composition into account, are more accurate and more precise (the variability in the relative error is also significantly smaller, $p < 0.001$), compared to age-depth models using simple linear interpolation. Furthermore, our experiment indicates that bulk sediment and *SARs* are well correlated. As such *BomDia* age-depth models have predictive power and may also assist in the evaluation of different tie-point scenarios for sediments older than the AMS $^{14}$C dating limit. In the section below, we illustrate how age-depth model uncertainty can be addressed using a Monte Carlo approach.

### 4.4. Evaluating Age-Depth Model Uncertainties Using a Monte Carlo Approach

Thus far, the *BomDia* script was used to interpolate ages between ACPs. However, the *BomDia* method also provides a powerful statistical tool for the testing of uncertainty in the age-depth model. We assess the age-depth model uncertainty using a Monte Carlo approach, which involves generation of a large number of randomly selected ACPs within the ACPs uncertainty intervals. In Figures 6 and 7, we show the result of a Monte Carlo simulation for core GeoB3910-2. We generated 500,000 age-depth models and isolated a small subset of 30 "best age-depth models", selected based upon minimum variability in the *CAR* parameter. In Figure 6c, we show the variability of the *CAR* parameter for the best solutions. Ideally, the variability between neighboring segments should overlap, which appears to be the case for most intervals. Some intervals in the upper part of the core, however, do not overlap with neighboring intervals. This indicates that there is not a single *CAR* value found
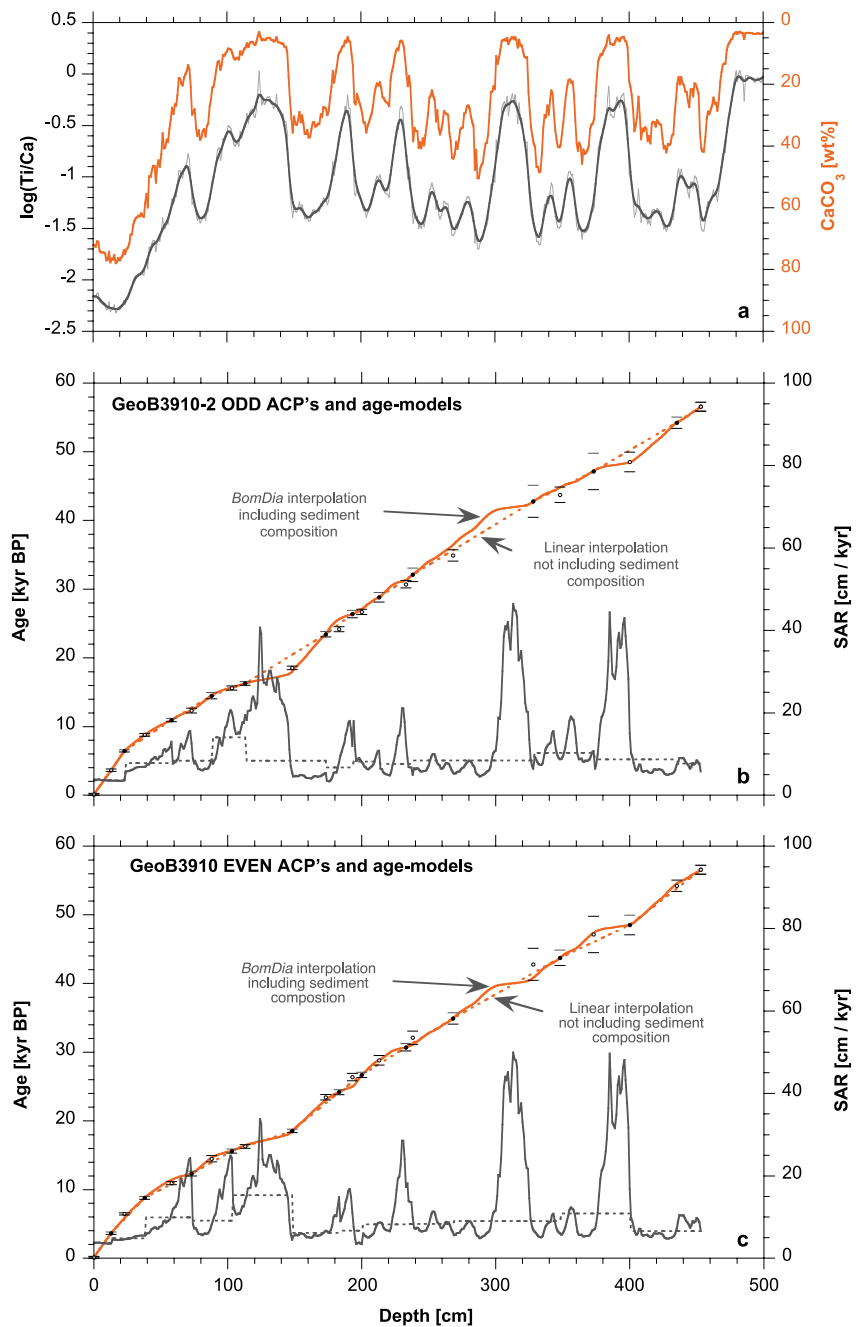
**Figure 4.** (a) The log(Ti/Ca) and CaCO$_3$ wt.%, plotted on reversed axis, for core GeoB3910-2. (b) Age models and sediment accumulation rate (*SAR*) for core GeoB3910-2 using the ODD sub-set of age control points (ACPs). The orange dashed line represents the linear age model, the solid orange line the *BomDia* age model. *SARs* for both age models are given in dark gray; dashed line for the linear model and solid line for the *BomDia* age model. The ACPs used for ODD subset of ACPs are given as solid dots including estimation of error (95% interval, see Table 1). The open circles are the unused ACPs of the other sub-set. (c) Same as in panel b, but now for the EVEN subset of ACPs. Offsets between the un-used ACPs and the age models are given in Table 1.

which offers an age-depth model solution for the two neighboring segments based upon a common *CAR* parameter value. These deviating intervals point to a (slightly) disturbed relationship between *SAR* and bulk sediment composition. We anticipate that these somewhat higher *CAR* values maybe due to less consolidated sediments upper part of the core or, alternatively, may be related to the effects of sea-level rise and shelf flooding, which could have changed the configuration of the regional depositional systems. In Figure 7a, we show the Monte
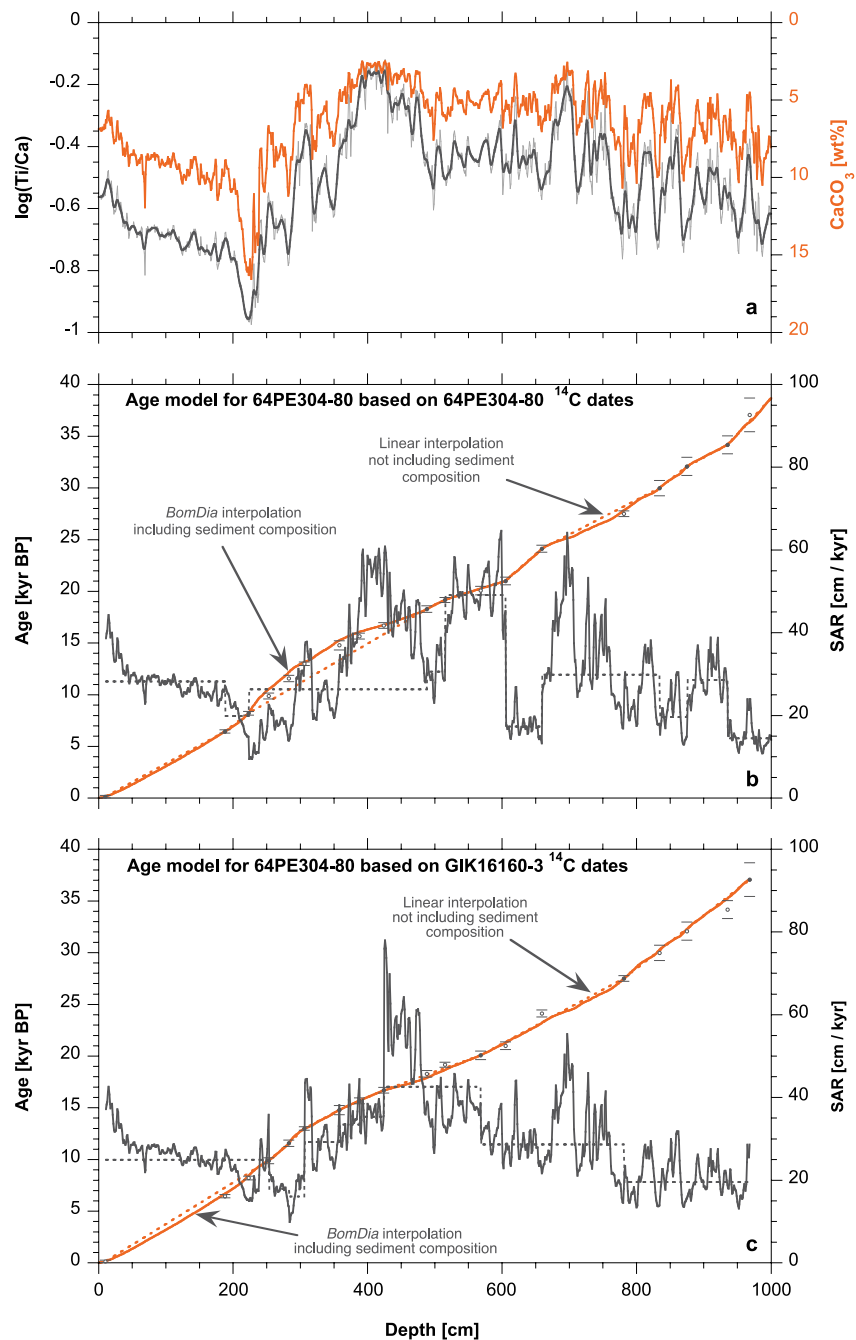
**Figure 5.** (a) The log(Ti/Ca) and CaCO₃ wt.%, plotted on reversed axis, for core 64PE304-80. (b) Age models and sediment accumulation rate (*SAR*) for core 64PE304-80 based upon 64PE304-80 AMS ^{14}C dates. The orange dashed line represents the linear age model, the solid orange line the *BomDia* age model. *SARs* for both age models are given in dark gray; dashed line for the linear model and solid line for the *BomDia* age model. The age control points (ACPs) used are measured on core 64PE304-80 and given as solid dots including estimation of error (95% interval, see Table 1). The open circles are the unused ACPs transposed from core GIK16160-3. (c) Same as panel b but now AMS ^{14}C dates used for the age models are from core GIK16160-3 and projected onto the depth of core 66PE304-80. Offsets between the un-used ACPs and the age models are given in Table 1.

Carlo age-depth model solution for the best 30 age-depth models and in Figure 7b, we show the two-sigma variability of these 30 Monte Carlo age-depth models. Given the relatively high density of AMS ^{14}C dates, the two-sigma uncertainty is low in the upper 200 cm of the core and is higher in the lower part of the core due to larger uncertainty in the AMS ^{14}C ages.
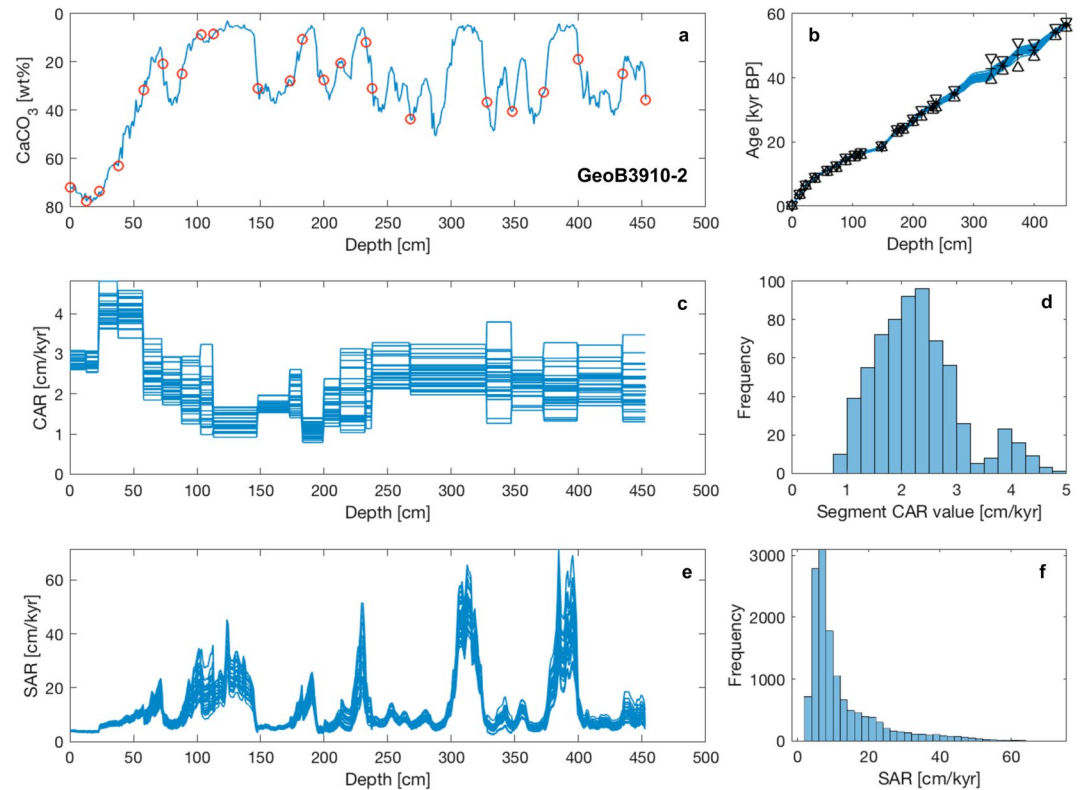
**Figure 6.** A full *BomDia* Monte Carlo age-depth model output for core GeoB3910-2 for 500,000 simulations, showing results for the 30 best Monte Carlo solutions (a) The CaCO₃ wt.% plotted versus depth in core. Position of age control points (ACPs) indicated by red circles. (b) Age-depth relationship for 30 best Monte Carlo age-depth models and ACPs with 3 s.d. uncertainty. (c) The variability in the down-core carbonate accumulation rate (*CAR*) segment values for 30 best solutions. (d) Frequency diagram of all *CAR* segment values for 30 best Monte Carlo age-depth models. (e) Sediment accumulation rates (*SARs*) for 30 best Monte Carlo age models. (f) Frequency diagram of *SAR*-values for the 30 best Monte Carlo age models.

In Figures 8 and 9, we show the results of the Monte Carlo simulation for core 64PE304-80. We generated 500,000 Monte Carlo models and consider the 30 best Monte Carlo age-depth models to provide an estimate of the uncertainty. In Figure 8c, we show that almost all *CAR* intervals overlap except an interval near 600 cm. A closer inspection, to detect deviating ACPs or hiatuses, thus appears necessary for this core. We discuss this further below.

## 5. Discussion

### 5.1. *BomDia*

The *BomDia* age-depth model algorithm includes information on bulk sediment composition when building age models for hemipelagic sediments. The algorithm essentially is an interpolation algorithm and it is able to assess age-depth model uncertainty using a MC approach. Estimates of uncertainty are useful in the decision-making process of the evaluation of age-depth models (Blaauw, 2010; Blaauw & Christen, 2011). In a simple experiment, we have shown that the *BomDia* algorithm performs significantly better than simple linear interpolation, which is commonly used to produce age-dept models for marine records, especially for models beyond the radiocarbon dating limit. In addition, the *BomDia* algorithm provides a powerful statistical tool to assess age-depth model robustness. To do so, statistical and visual evaluation of the age-depth model may be performed through the analysis of the model parameter (*CAR*). Below we further discuss on how this may be performed.

### 5.2. The *CAR* Parameter and Recognition of Outlier ACPs

The *BomDia* algorithm allows for the quick generation of age-depth models for various sets of ACPs. For each segment, an interval bounded by two ACPs, the model outputs multiple estimates of the *CAR* parameter. For a
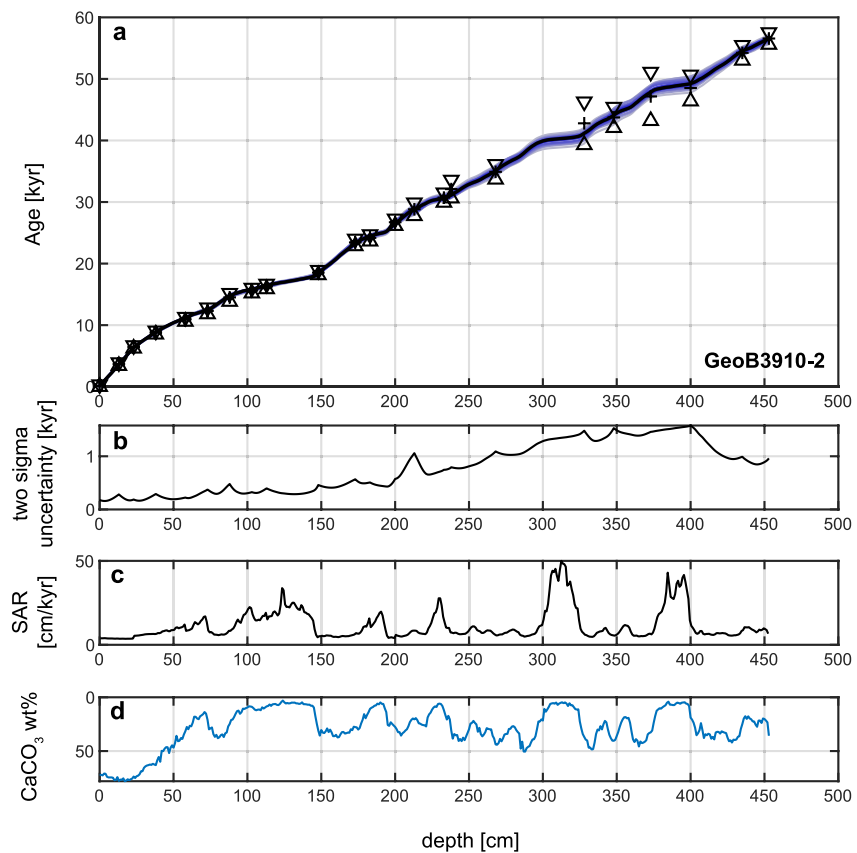
**Figure 7.** (a) A *BomDia* Monte Carlo age-depth model output for 500,000 simulations for core GeoB3910-2. Output shown is the "median" *BomDia* age-depth model (black line) based upon the 30 best Monte Carlo simulations with lowest carbonate accumulation rate parameter variability (shown in Figure 6c). Percentile shading (in blue) indicates 5%–95% percentiles in steps of 5%. The AMS $^{14}C$ median ages and 3-sigma uncertainty are indicated by crosses and triangles, respectively. (b) Two sigma variability ("uncertainty") of the 30 best Monte Carlo age models. (c) The sediment accumulation rate (median age-depth model). (d) The CaCO$_3$ wt.% for core GeoB3910-2, reflecting bulk sediment composition, is plotted on reversed axis.

core with $k$ ACPs, there are $k − 1$ segments of the *CAR* parameter produced. The *CAR* parameter, which is considered to reflect the pelagic carbonate accumulation component of lithogenic free sediment, is expected to vary between ~1 and 5 cm/kyr (Olson et al., 2016; Piper, 2005). Once a histogram of *CAR* values has been produced for a given record, one may use the downcore evolution and (statistical) characteristics of the *CAR* parameter distribution to detect potential outliers in the ACPs. In Figures 6 and 8, a full graphical output of the *BomDia* algorithm script for cores GeoB3910-2 and 64PE304-80 is shown, using all available AMS $^{14}C$ dates (Table 1). The distribution of *CAR* values is shown versus depth in Figures 6c and 8c, and as a histogram in Figures 6d and 8d. To evaluate the age-depth model for potential irregularities, we examine the downcore evolution of *CAR* values. For core GeoB3910-2 (Figure 6c), the variability in the *CAR* values for most segments overlaps with their neighboring segments. As such, a change in the *CAR* parameter from one segment to the next is considered to occur within error. Some segments, however, do not overlap with neighboring segments, as is the case in the upper part of the core, that is, for the third and the forth segments. These segments show relatively high values and fail to overlap with their neighboring (i.e., the second and fifth) segments. Apparently, the relationship between bulk sedimentology and *CAR* values is somewhat disturbed. As discussed above, these higher than expected *CAR* values may point to less consolidated sediments in the upper part of the record, or related to changes the depositional system due to sea-level rise and shelf flooding. Furthermore, between ~200 and 100 cm, the age of the sediment is between ~26.6 and 15.5 ka, and *CAR* values appear somewhat lower compared to the rest of the record. Although a unique explanation cannot be given, the lower values may reflect a change in the depositional setting resulting from a relatively low sea-level, or they may result from a somewhat lower than average carbonate production during full glacial conditions in the tropical Atlantic Ocean (Catubig et al., 1998). A closer look at the
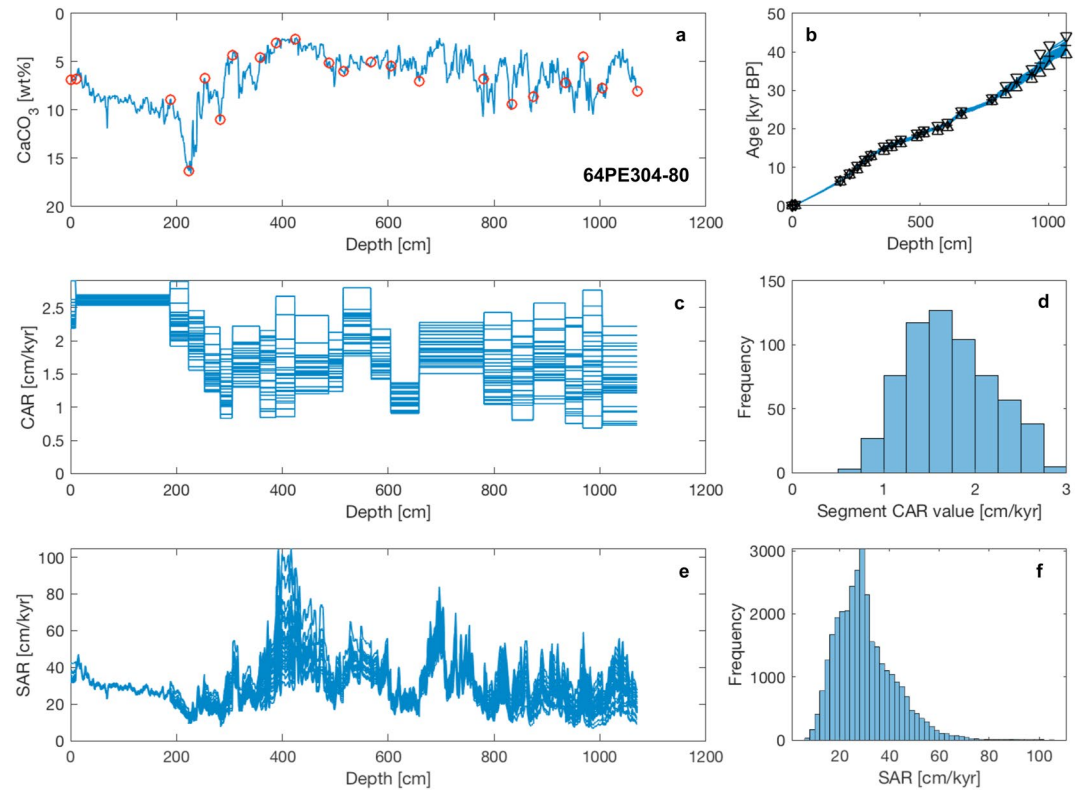
**Figure 8.** A full *BomDia* Monte Carlo age-depth model output for core 64PE304-80 for 500,000 simulations, showing results for the 30 best Monte Carlo solutions (a) The CaCO_3 wt.% plotted versus depth in core. Position of age control points (ACPs) indicated by red circles. (b) Age depth relationship for 30 best Monte Carlo age-depth models and ACPs with 3 s.d. uncertainty. (c) The variability in the down-core carbonate accumulation rate (*CAR*) segment values for 30 best solutions. (d) Frequency diagram of all *CAR* segment values for 30 best Monte Carlo age models. (e) Sediment accumulation rates (*SARs*) for 30 best Monte Carlo age models. (f) Frequency diagram of *SAR*-values for the 30 best Monte Carlo age-depth models.

*CAR* values for core 64PE304-80 (Figure 8c) also shows that the variability in the *CAR* segment values generally overlaps from one interval to the next. One interval, between 659 and 605 cm, however, stands out. The deviating low *CAR* values do not overlap in range with the neighboring intervals. Although the values from this interval appear to fit in the overall distribution of *CAR* values for the entire core (Figure 8d), the transient development suggest a relatively poor age assessment for the AMS ^{14}C date at 659 cm. As such, removal of this ACP in the construction of the final age-depth model should be considered. We conclude that studying and understanding the *CAR* parameter distribution provides a powerful (statistical) tool in detecting potentially deviating ACPs. Whereas the long-term ($10^3$–$10^4$ yr) evolution of the *CAR* parameter is considered to reflect long-term changes in carbonate production, more abrupt shifts, which cannot be explained by ACP uncertainty, may reflect variation in the degree of compaction of the sediments, reflect changes in depositional system related to sea-level, or point to core stretching in case *CAR* values are higher than expected. On the other hand, an exceptional lower than expected *CAR* segment value, may point to period of low sediment accumulation or to a hiatus.

### 5.3. Prediction of ACPs and Reduction of Age-Depth Model Uncertainty

An independent age-depth model with realistic sedimentation rates in line with sedimentological development, such as presented in this study, is a prerequisite in understanding tele-connections between different paleoclimate proxy records. ACPs based on AMS ^{14}C dating are inherently subject to uncertainty. Quantification of various sources of uncertainty including the effects of bioturbation on downcore age heterogeneity (Dolman et al., 2021) will help to produce the most optimal age-depth model for a given record. The *BomDia* algorithm benefits from realistic age-uncertainty estimates and generally produces smoother age-depth models, that is, with lower down-core *CAR* parameter variability, when uncertainty of the ACPs is raised. Raising the uncertainty of the ACPs, however, comes at the price of raised uncertainty in the age model.
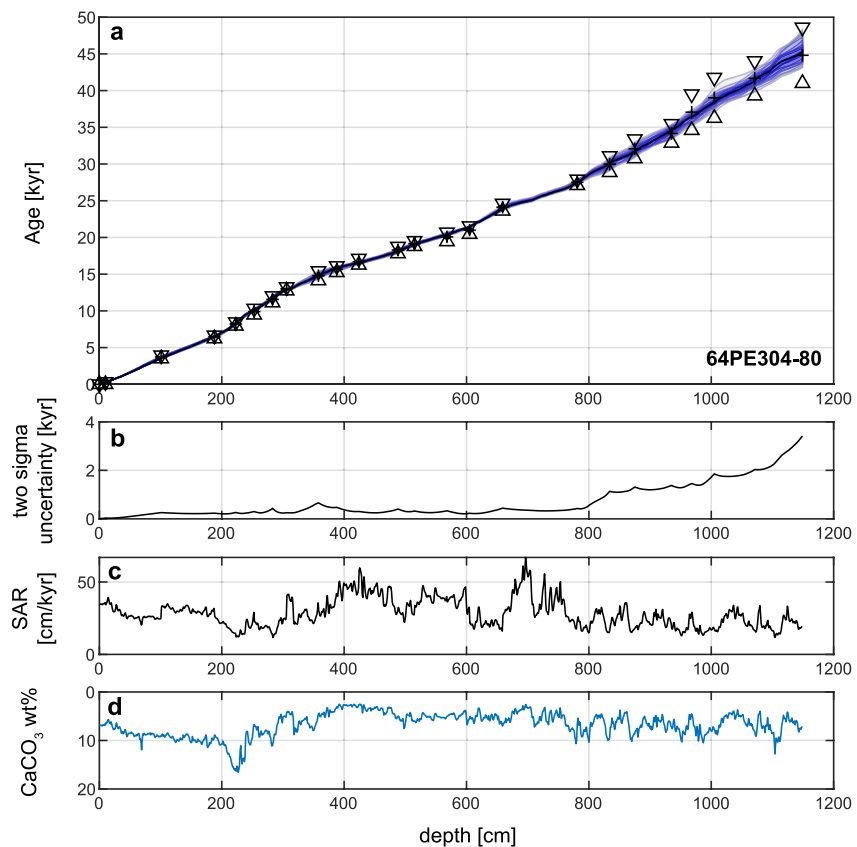
**Figure 9.** (a) A *BomDia* Monte Carlo age-depth model output for 500,000 simulations for core 64PE304-80. Output shown is the "median" *BomDia* age-depth model (black line) based upon the 30 best Monte Carlo simulations with lowest carbonate accumulation rate parameter variability (shown in Figure 8c). The AMS $^{14}$C median ages and 3-sigma uncertainty are indicated by crosses and triangles, respectively. (b) Two sigma variability ("uncertainty") of the 30 best Monte Carlo age models. (c) The sediment accumulation rate (median age-depth model). (d) The CaCO$_3$ wt.% for core 64PE304-80, reflecting bulk sediment composition, is plotted on reversed axis.

Age-depth models for sediments older than the AMS $^{14}$C dating limit, generally rely on tuning strategies to other paleo-climatic records with trusted chronologies. Tuning mistakes may be made easily and fuel scientific debate (e.g., Auer et al., 2020). Here, the *BomDia* algorithm/approach may assist in the decision-making process of different tuning strategies. Once a robust estimate of the relationship between bulk sediment composition and *SARs* for a given site has been established, this relationship may be used to predict ages of the tie-points used. As such, different tuning strategies may be evaluated. We expect that this approach will lead to a further reduction of age-depth model uncertainty.

### 5.4. Wider Applicability of *BomDia*?

The *BomDia* approach utilizes the CaCO$_3$ wt.% of sediments as a proxy for *SAR*. To produce an age-depth model at high XRF resolution, we here estimate CaCO$_3$ wt.% from high-resolution XRF derived log(Ti/Ca) (Figure 2). The dilution effect of the pelagic calcium carbonate fraction, caused by variation in terrigenous input, forms the basis for the algorithm. It is important to note that the algorithm is expected to perform less optimal when sediments are disturbed, sorted by deep-sea currents ("winnowing") or have been subject to carbonate dissolution. It is therefore advisable to only use the algorithm for well-preserved marine hemipelagic sediments that have been deposited above the carbonate compensation depth. Another potential complication in the applicability may appear in case the terrigenous fraction also contains carbonates. Marine records under the influence of Saharan dust, for example, may contain some portion of autochthonous biogenic carbonates (Moreno et al., 2006), which in turn may potentially influence the effectiveness of the log(Ti/Ca) as a proxy for the terrestrial versus pelagic marine fractions. Although we have not investigated this aspect here, the application of the method to sediment

cores from sub-polar and polar latitudes may be complicated by the presence of ice rafted debris (IRD). We expect that the presence of IRD will disturb the relationship between log(Ti/Ca) and *SAR*. Potentially visual quantification of IRD and or other elemental ratios may be considered when building age-depth models with *BomDia*. Future versions of our algorithm may be extended to include some of the complicating processes described above.

## 6. Conclusion

We have shown that including XRF-based bulk sediment composition significantly improves the accuracy and predictive quality of age-depth models for tropical marine hemipelagic records. An age-depth model algorithm, referred to as "*BomDia*", has been developed for this purpose. We show that when sediment composition is incorporated into the age-depth modeling procedure, the predictive quality of the age-depth model (i.e., the relative error of prediction) significantly improves compared to simple linear interpolation. The model uses only one parameter which is calculated for individual core segments. We refer to this parameter as the *CAR*, which mirrors the terrigenous clastic-free accumulation rate of the sediment. The probability distribution of the *CAR* parameter and its transient down-core development, provide a powerful statistical tool for the testing of the robustness of the age-depth model, including detection of hiatuses and/or detection of intervals with questionable *SARs*. Uncertainty in the age-depth model is addressed using a Monte Carlo approach, which takes into account the uncertainty associated with the ACPs. Finally, the *BomDia* approach is expected to prove useful in the testing of different tuning strategies for marine paleoclimate time series older than the radiocarbon dating limit of ~50 ka.

## Conflict of Interest

The authors declare no conflicts of interest relevant to this study.

## Data Availability Statement

The AMS $^{14}$C data used in this study for cores GeoB3910-2 and 64PE304-80 can be found in Jaeschke et al. (2007a, 2007b, Table 1) and van der Lubbe et al. (2016, Table 1). Re-calibrated AMS $^{14}$C data for cores GeoB3910-2 and 64PE304-80 are shown in Table 1 (this study). The *MatCal* algorithm (Lougheed & Obrochta, 2016) used for the AMS $^{14}$C re-calibration is available via https://github.com/bryanlougheed/MatCal/. The Ti/Ca data associated with cores GeoB3910-2 and 64PE304-80 are available via Pangaea Data Publisher for Earth and Environmental Science (Jaeschke et al., 2007a; van der Lubbe, 2022a). The calcium carbonate data associated with core GIK16160-3 are available via Pangaea Data Publisher for Earth and Environmental Science (van der Lubbe, 2022b). The *BomDia.m* algorithm, the function *getcar.m* and input files discussed in this paper are available via Zenodo (Peeters, 2022).

## References

Arz, H. W., Pätzold, J., & Wefer, G. (1998). Correlated millennial-scale changes in surface hydrography and terrigenous sediment yield inferred from last-glacial marine deposits off northeastern Brazil. *Quaternary Research*, *50*(2), 157–166. https://doi.org/10.1006/qres.1998.1992

Arz, H. W., Pätzold, J., & Wefer, G. (1999). Climatic changes during the last deglaciation recorded in sediment cores from the northeastern Brazilian Continental Margin. *Geo-Marine Letters*, *19*(3), 209–218. https://doi.org/10.1007/s003670050111

Auer, G., de Vleeschouwer, D., & Christensen, B. A. (2020). Toward a robust Plio-Pleistocene chronostratigraphy for ODP Site 762. *Geophysical Research Letters*, *47*(3). https://doi.org/10.1029/2019GL085198

Behling, H., Arz, H. W., Pätzold, J., & Wefer, G. (2000). Late Quaternary vegetational and climate dynamics in northeastern Brazil, inferences from marine core GeoB 3104-1. *Quaternary Science Reviews*, *19*(10), 981–994. https://doi.org/10.1016/S0277-3791(99)00046-3

Blaauw, M. (2010). Methods and code for "classical" age-modeling of radiocarbon sequences. *Quaternary Geochronology*, 5, 512–518. https://doi.org/10.1016/j.quageo.2010.01.002

Blaauw, M. (2012). Out of tune: The dangers of aligning proxy archives. *Quaternary Science Reviews*, *36*, 38–49. https://doi.org/10.1016/j.quascirev.2010.11.012

Blaauw, M., & Christen, A. J. (2011). Flexible paleoclimate age-depth models using an autoregressive gamma process. *Bayesian Analysis*, *6*(3), 457–474. https://doi.org/10.1214/11-BA618

Bronk Ramsey, C. (2009). Bayesian analysis of radiocarbon dates. *Radiocarbon*, *51*(1), 337–360. https://doi.org/10.1017/S0033822200033865

Burckel, P., Waelbroeck, C., Gherardi, J. M., Pichat, S., Arz, H., Lippold, J., et al. (2015). Atlantic Ocean circulation changes preceded millennial tropical South America rainfall events during the last glacial. *Geophysical Research Letters*, *42*(2), 411–418. https://doi.org/10.1002/2014GL062512

Catubig, N. R., Archer, D. E., Francois, R., de Menocal, P., Howard, W., & Yu, E.-F. (1998). Global deep-sea burial rate of calcium carbonate during the last glacial maximum. *Paleoceanography*, *13*(3), 298–310. https://doi.org/10.1029/98PA00609

Chiessi, C. M., Mulitza, S., Taniguchi, N. K., Prange, M., Campos, M. C., Haggi, C., et al. (2021). Mid- to Late Holocene contraction of the intertropical convergence zone over northeastern South America. *Paleoceanography and Paleoclimatology*, *36*(4), e2020PA003936. https://doi.org/10.1029/2020PA003936

Crundwell, M. P. (2016). A new method for interpolating ages between calibrated control points based on foraminiferal concentrations. *Journal of Sedimentary Research*, *86*(5), 438–447. https://doi.org/10.2110/jsr.2016.34

Dolman, A. M., Groeneveld, J., Mollenhauer, G., Ho, S. L., & Laepple, T. (2021). Estimating bioturbation from replicated small-sample radiocarbon ages. *Paleoceanography and Paleoclimatology*, *36*(7), e2020PA004142. https://doi.org/10.1029/2020PA004142

Fütterer, D. K. (2006). The solid phase of marine sediments. In H. D. Schulz, & M. Zabel (Eds.), *Marine geochemistry* (pp. 1–25). Springer Berlin. https://doi.org/10.1007/978-3-662-04242-7

Govin, A., Capron, E., Tzedakis, P., Verheyden, S., Ghaleb, B., Hillaire-Marcel, C., et al. (2015). Sequence of events from the onset to the demise of the Last Interglacial: Evaluating strengths and limitations of chronologies used in climatic archives. *Quaternary Science Reviews*, *129*, 1–36. https://doi.org/10.1016/j.quascirev.2015.09.018

Hennekam, R., & de Lange, G. (2012). X-Ray fluorescence core scanning of wet marine sediments: Methods to improve quality and reproducibility of high-resolution paleoenvironmental records. *Limnology and Oceanography: Methods*, *10*(12), 991–1003. https://doi.org/10.4319/lom.2012.10.991

Herterich, K., & Sarnthein, M. (1984). Bruhnes time scale: Tuning by rates of calcium-carbonate dissolution and cross spectral analysis with solar insolation. In A. L. Berger (Ed.), *Milankovitch and climate, Part 1* (pp. 447–466). D. Reidel Publishing Company.

Hodell, D., Crowhurst, S., Skinner, L., Tzedakis, P. C., Margari, V., Channell, J. E. T., et al. (2013). Response of Iberian Margin sediments to orbital and suborbital forcing over the past 420 ka. *Paleoceanography*, *28*(1), 185–199. https://doi.org/10.1002/palo.20017

Jaeschke, A., Rühlemann, C., Arz, H. W., Heil, G. M. N., & Lohmann, G. (2007a). Titanium/Calcium ratios of sediment core GeoB3910-2 from the northeastern Brazil continental slope [Dataset]. PANGAEA. https://doi.org/10.1594/PANGAEA.667497

Jaeschke, A., Rühlemann, C., Arz, H. W., Heil, G. M. N., & Lohmann, G. (2007b). Coupling of millennial-scale changes in sea surface temperature and precipitation off northeastern Brazil with high-latitude climate shifts during the last glacial period. *Paleoceanography*, *22*(4). https://doi.org/10.1029/2006PA001391

Lisiecki, L. E., & Raymo, M. E. (2005). A Pliocene-Pleistocene stack of 57 globally distributed benthic d$^{18}$O records. *Paleoceanography*, *20*(1), PA1003. https://doi.org/10.1029/2004PA001071

Lougheed, B. C., & Obrochta, S. P. (2016). MatCal: Open source Bayesian $^{14}$C age calibration in Matlab. *Journal of Open Research Software*, *4*(1), e42. https://doi.org/10.5334/jors.130

Lougheed, B. C., & Obrochta, S. P. (2019). A rapid, deterministic age-depth modeling routine for geological sequences with inherent depth uncertainty. *Paleoceanography and Paleoclimatology*, *34*(1), 122–133. https://doi.org/10.1029/2018PA003457

Martinson, D. G., Pisias, N. G., Hays, J. D., Imbrie, J., Moore, T. C., & Shackleton, N. J. (1987). Age dating and the orbital theory of the ices age: Development of a high-resolution 0–300,000 yr chronostratigraphy. *Quaternary Research*, *27*, 1–29. https://doi.org/10.1016/0033-5894(87)90046-9

Moreno, T., Querol, X., Castillo, S., Alastuey, A., Cuevas, E., Herrmann, L., et al. (2006). Geochemical variations in aeolian mineral particles from the Sahara-Sahel dust corridor. *Chemosphere*, *65*(2), 261–270. https://doi.org/10.1016/j.chemosphere.2006.02.052

Olson, P., Reynolds, E., Hinnov, L., & Goswami, A. (2016). Variation of ocean sediment thickness with crustal age. *Geochemistry, Geophysics, Geosystems*, *17*(4), 1349–1369. https://doi.org/10.1002/2015GC006143

Peeters, F. J. C. (2022). fjcpeeters/*BomDia*: *BomDia* (Version 3.0) [Software]. Zenodo. https://doi.org/10.5281/zenodo.7142941

Piper, D. J. W. (2005). Sedimentary processes|deep water processes and deposits. In R. C. Selley, L. R. M. Cocks, & I. R. Plimer (Eds.), *Encyclopedia of geology* (pp. 641–649). Elsevier.

Reimer, P. J., Austin, W. E. N., Bard, E., Bayliss, A., Blackwell, P. G., Bronk Ramsey, C., et al. (2020). The IntCal20 Northern Hemisphere radiocarbon age calibration curve (0–55 cal kBP). *Radiocarbon*, *62*(4), 725–757. https://doi.org/10.1017/RDC.2020.41

Schefuss, E., Kuhlmann, H., Mollenhauer, G., Prange, M., & Pätzold, J. (2011). Forcing of wet phases in southeast Africa over the past 17,000 yr. *Nature*, *480*(7378), 509–512. https://doi.org/10.1038/nature10685

Scussolini, P., Peeters, F. J. C., Arz, H., Kaiser, J., Dokken, T. M., Waelbroeck, C., & Renssen, H. (2014). Anti-phasing of northern and Southern Hemisphere monsoons during the past 420,000 yr. In P. Scussolini (Ed.), *Dynamics of Pleistocene climate change in the South Atlantic Ocean* (pp. 91–127). Vrije Universiteit Amsterdam.

Skonieczny, C., McGee, D., Winckler, G., Bory, A., Bradtmiller, L. I., Kinsley, C. W., et al. (2019). Monsoon-driven Saharan dust variability over the past 240,000 yr. *Science Advances*, *5*(1), eaav1887. https://doi.org/10.1126/sciadv.aav1887

Telford, R. J., Heegaard, E., & Birks, H. J. B. (2004). All age-depth models are wrong: But how badly? *Quaternary Science Reviews*, *23*(1–2), 1–5. https://doi.org/10.1016/j.quascirev.2003.11.003

Trachsel, M., & Telford, R. J. (2017). All age-depth models are wrong, but are getting better. *The Holocene*, *27*(6), 860–869. https://doi.org/10.1177/0959683616675939

van der Lubbe, H. J. L., Frank, M., Tjallingii, R., & Schneider, R. R. (2016). Neodymium isotope constraints on provenance, dispersal, and climate-driven supply of Zambezi sediments along the Mozambique Margin during the past ~45,000 yr. *Geochemistry, Geophysics, Geosystems*, *17*(1), 181–198. https://doi.org/10.1002/2015GC006080

van der Lubbe, H. J. L., Tjallingii, R., Prins, M. A., Brummer, G.-J. A., Jung, S. J. A., Kroon, D., & Schneider, R. R. (2014). Sedimentation patterns of the Zambezi River over the last 20,000 yr. *Marine Geology*, *355*, 189–201. https://doi.org/10.1016/j.margeo.2014.05.012

van der Lubbe, J. (2022a). Calcium and titanium counts of sediment core 64PE304-80 from Mozambique Margin [Dataset]. PANGAEA. https://doi.org/10.1594/PANGAEA.953079

van der Lubbe, J. (2022b). Calcium carbonate, organic content and calcium and titanium counts of sediment core GIK16160-3 from Mozambique Margin [Dataset]. PANGAEA. https://doi.org/10.1594/PANGAEA.953081

Waelbroeck, C., Lougheed, B. C., Vazquez Riveiros, N., Missiaen, L., Pedro, J., Dokken, T., et al. (2019). Consistently dated Atlantic sediment cores over the last 40,000 yr. *Scientific Data*, *6*(1), 165. https://doi.org/10.1038/s41597-019-0173-8

Weltje, G. J., & Tjallingii, R. (2008). Calibration of XRF core scanners for quantitative geochemical logging of sediment cores: Theory and application. *Earth and Planetary Science Letters*, *274*(3–4), 423–438. https://doi.org/10.1016/j.epsl.2008.07.054